SCIENTIFIC REPORTS

OPEN

SUBJECT AREAS:
MATERIALS SCIENCE
NANOSCALE MATERIALS
GRAPHENE
SYNTHESIS OF GRAPHENE

Received
18 June 2012

Accepted
9 January 2013

Published
28 January 2013

Correspondence and requests for materials should be addressed to S.M. (msc@whut.edu.cn)

Direct Transformation of Amorphous Silicon Carbide into Graphene under Low Temperature and Ambient Pressure

Tao Peng, Haifeng Lv, Daping He, Mu Pan & Shichun Mu

State Key Laboratory of Advanced Technology for Materials Synthesis and Processing, Wuhan University of Technology, Wuhan 430070, PR China.

A large-scale availability of the graphene is critical to the successful application of graphene-based electronic devices. The growth of epitaxial graphene (EG) on insulating silicon carbide (SiC) surfaces has opened a new promising route for large-scale high-quality graphene production. However, two key obstacles to epitaxial growth are extremely high requirements for almost perfectly ordered crystal SiC and harsh process conditions. Here, we report that the amorphous SiC (a-$Si_{1-x}C_x$) nano-shell (nano-film) can be directly transformed into graphene by using chlorination method under very mild reaction conditions of relative low temperature (800°C) and the ambient pressure in chlorine (Cl_2) atmosphere. Therefore, our finding, the direct transformation of a-$Si_{1-x}C_x$ into graphene under much milder condition, will open a door to apply this new method to the large-scale production of graphene at low costs.

Graphene, owing to its novel magnetotransport properties[1–3], high carrier mobility and ballistic transport up to room temperature[4], has attracted enormous attention since its discovery in 2004[5]. To harness these properties for applications, large-scale synthesis is urgently required. Several methods for graphene production have been proposed. Micromechanical cleavage was used to make graphene[5]. However, it is difficult to scale up this process to large-scale production. Alternatively, graphene is also usually achieved by using dispersion and exfoliation of graphene oxide[6]. However, the graphene oxide is significant different from graphene[7]. Although it can be reduced to remove the redundant functional groups, this inevitably contributes to a significant number of defects as well as a quite complicated process[7]. Graphene can be grown on the surface of transition metals such as Ru (0001)[8], but this method requires transfer of the resulting graphene to another substrate to make useful devices. Recently, growth of graphene has been fulfilled by graphitization of SiC substrates[9–12]. The epitaxial growth methods bring us to very new world for producing graphene. However, large-scale production of graphene via epitaxial growth methods is significantly hindered by extremely high requirements for almost perfectly ordered crystal SiC and harsh process condition[10] including high temperature (>1200°C) and ultra-high vacuum (UHV). Thus, a new facile method for graphene preparation is urgently required, and the perfectly ordered crystal SiC must be substituted by the large availability of cheap raw materials.

Graphite, carbon onions and graphene nanosheets were generated as the by-products in synthesizing Carbide-derived carbons (CDCs) in halogen atmosphere at the ambient pressure, but the significant graphitization of carbide precursors (SiC, SiOC, TiC, Ti_3SiC_2, etc.) only occurred at the temperature higher than 1200°C[13,14]. Furthermore, it has been found that the introduction of defects could lower the energy barrier for the precursor conversion into the more stable forms[15]. Therefore, it is strongly expected that the high synthesis temperature and the UHV requirements can be significantly alleviated by utilizing long-range disordered amorphous carbide precursors that are defect-rich (see Supplementary Fig. S1 online). The isotropic a-$Si_{1-x}C_x$ is cheap and it can be easily synthesized via many ways[16]. Moreover, it might not require highly oriented for growing epitaxial graphene, and its morphology and composition (such as x value) can be effectively tuned during synthesis process[16]. However, to our best knowledge, no effort has been tried so far to exploit a-$Si_{1-x}C_x$ as the graphene synthesis precursor. Here, we firstly report a facile method for graphene preparation using a-$Si_{1-x}C_x$ under much milder process conditions by a chlorination method.

Results

To determine the transformation of a-$Si_{1-x}C_x$ nano-shell on SiC nano-particles into graphene, the HRTEM images and Raman spectroscopy are given in Fig. 1. The typical HRTEM images of as-received nano-SiC and

prepared SiC-CDC are shown in Fig. 1a and b, respectively. All SiC nanoparticles with β-SiC core were surrounded by a-$Si_{1-x}C_x$ nano-shells with thickness of less than 10 nm (Fig. 1a). The resulting amorphous carbon nano-particles, as shown in the inset of Fig. 1b, kept almost the same shape and volume as those of the starting SiC, being consistent with the conformal transformation[13]. However, the green and blue circled areas in Fig. 1b show significantly different morphology, which can be readily found out through the entire SiC-CDC sample. In order to confirm the variety of morphologies, we magnified these circled areas. Quite significantly, some obviously detached graphene (Fig. 1c) with few layers (from two to eight layers) can be identified, and in particular, some β-SiC and amorphous carbon nano-particles were covered by epitaxial graphene (EG) (Fig. 1d and e). The EG was probably formed via the transformation of a-$Si_{1-x}C_x$ nano-shell, for the amorphous carbon that produced from a-$Si_{1-x}C_x$ nano-shell conversion, according to the conformal transformation[13,14], could form nano-shell over the nano-particle surface. Therefore, we come to believe that the detached graphene (Fig. 1c) was one type of epitaxial graphenes (EGs), which was generated from the a-$Si_{1-x}C_x$ nano-shell conversion and surprisingly be stripped off from the nano-particle surface. The detachment of the graphene layers from the SiC nano-particles indicates that the cohesive strength of the EG/SiC interface might not be very strong.

The Raman spectrum of the SiC-CDC (SiC) is shown in Fig. 1f. The longitudinal optical (LO) and transverse optical (TO) peaks indicate the presence of β-SiC phase[17]. No graphite and graphene can be detected in the SiC nano-particles (see Supplementary Fig. S2 a, b and c online). However, the occurrence of 2D, D + G and the two relatively large D and G peaks at 1340 and 1590 cm^{-1} indicates presence of the ordered graphitic domains in a-$Si_{1-x}C_x$ network[16,18]. Although only a small amount of a-$Si_{1-x}C_x$ was found compared with β-SiC phase (Fig. 1a), the intensities of the D and G peaks were even higher than that of LO and TO peaks, which can be ascribed to the significantly greater C-C bond Raman efficiency than that of the Si-C bond[18]. The C-C bonds may impose significant impacts on the structure of the produced SiC-CDC[13,14].

The SiC-CDC nano-particles after chlorination show the weak LO and TO peaks probably due to the presence of residual β-SiC (Fig. S3). Although the intensities of the D peak sharply increase, the surprising decrease of I_D/I_G ratio after chlorination exhibits the existence of larger crystalline size or a higher graphitization degree[19,20], which is consistent with the decrease of D peak normalized by the intensity of G-peak (in the inset of Fig. 1f). Although, the intensity of the 2D peak is relatively low owing to the relatively low content of graphene in the SiC-CDC nano-particles, profoundly, the 2D peak of SiC-CDC, consisting of two peaks $2D_1$ (2669 cm^{-1}) and $2D_2$

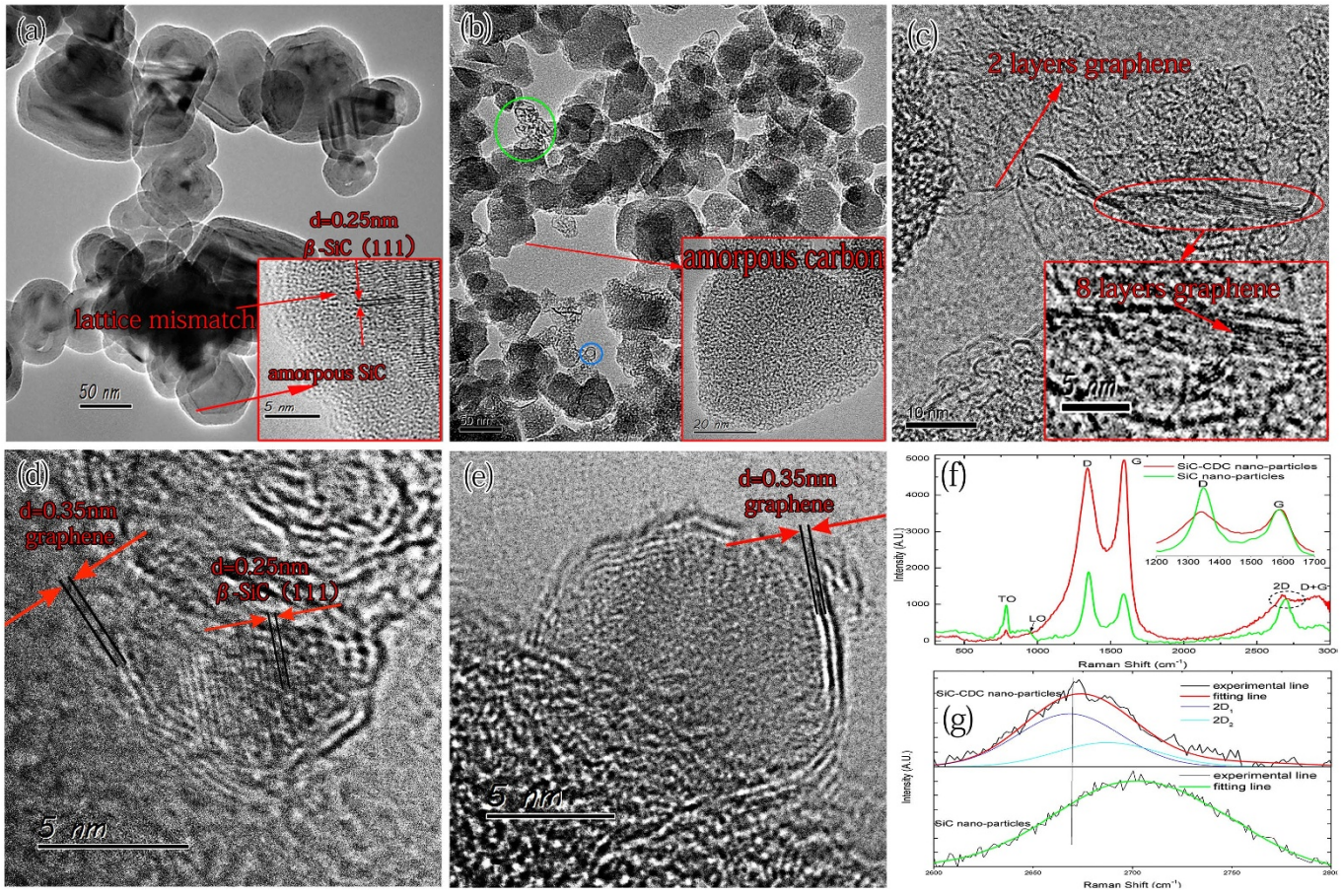

Figure 1 | (a) The SiC nano-particle HRTEM image. The a-$Si_{1-x}C_x$ alloys nano-shells are clearly evident. (b) The HRTEM image of SiC-CDC nano-particles after SiC chlorination. (c) The magnified image of the green circled area in (b) showing the EG that stripped from the substrate. The common length of resulting graphene from SiC-CDC nano-particles is less than 50 nm. (d), (e) The magnified images of the blue circled area in (b) showing the EG that adhere to β-SiC or amorphous carbon. (f) Raman-scattering spectra from SiC and SiC-CDC nano-particles. The G and D peaks, normalized by the intensity of G-peak in the inset, show decrease of D-peak, which is consistent with the decrease of I_D/I_G ratio. (g) Magnification of the 2D line in (f) showing the down-shifting of the 2D-peak after SiC chlorination. The peak fit of the $2D_1$ and $2D_2$ components to the 2D SiC-CDC band is shown. All peaks are amplitude normalized and vertically offset. The single SiC peak is at around 2702 cm^{-1}. The two inner most SiC-CDC peaks, i.e., $2D_1$ and $2D_2$, are at 2669 and 2688 cm^{-1}, respectively. The down-shifting of 2D SiC-CDC peak and the relatively strong $2D_1$ peak further confirms the graphene formation.

(2688 cm^{-1}), has been down-shifted of 29 cm^{-1} compared with around 2702 cm^{-1} of SiC (Fig. 1g). It is well known that a further decrease in layer numbers of graphene can lead to a significant increase in the relative intensity of $2D_1$ peaks[21–24]. In particular, the monolayer graphene has much narrower and down-shifting 2D band as compared with the multi-layer graphenes[23,25,26]. Therefore, the down-shifting of 2D SiC-CDC peak and the relatively strong $2D_1$ peak further confirms the formation of graphene.

In order to expose the graphene wrapped by amorphous carbon, the electrochemical erosion (ECE) technique was conducted to strip off the amorphous carbon on the surface of the SiC-CDC nano-particles. The cyclic voltammograms of the SiC-CDC samples

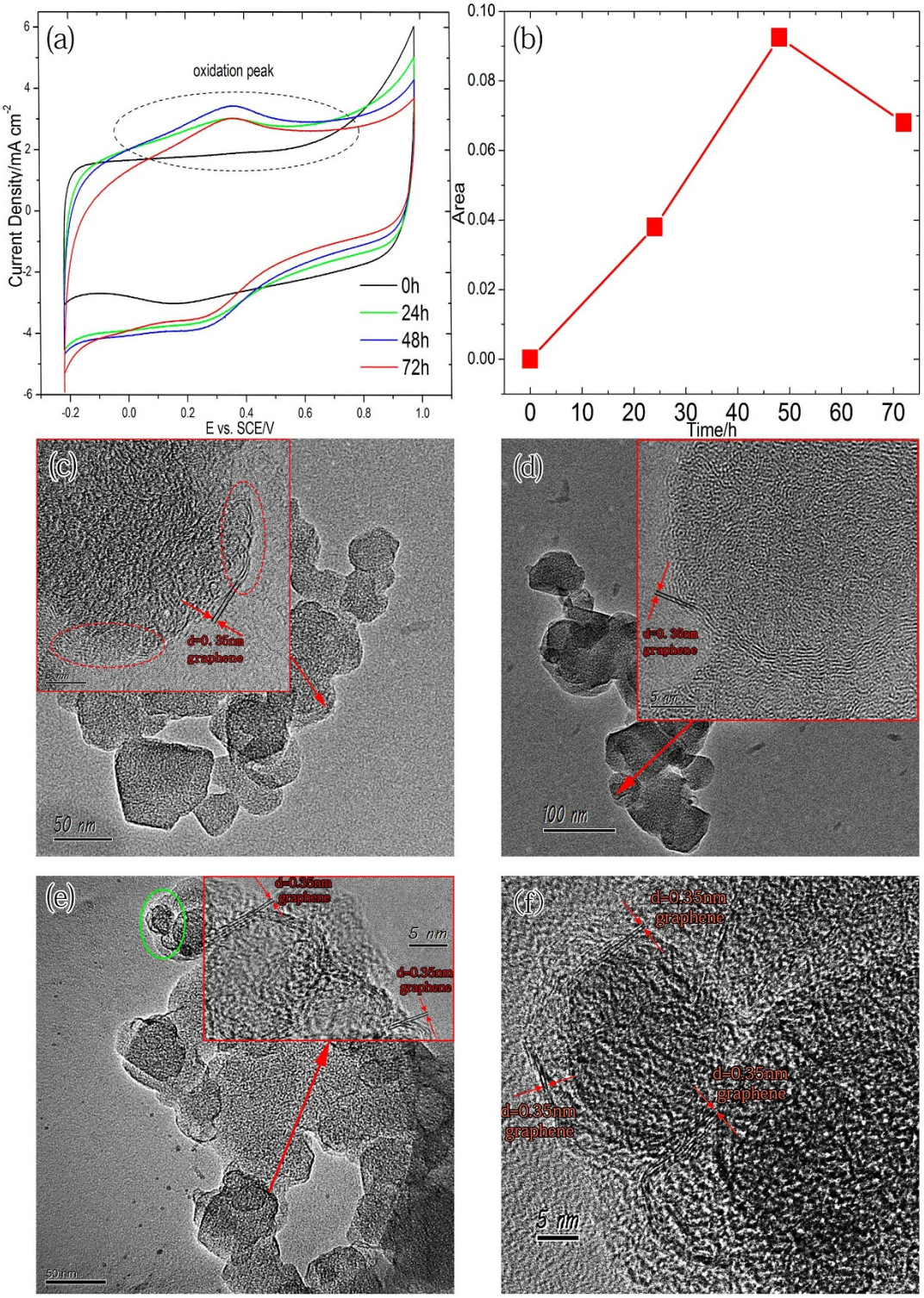

Figure 2 | (a) CV plots of SiC-CDC nanoparticles treated by ECE technique under a voltage of 0.98 V over different periods (0.5 M H_2SO_4, scan rate: 50 mVs−1). (b) The oxidation peak areas were quantitatively obtained by integrating the region enclosed by the cathode scan curve above the double layer charge region. (c), (d) and (e) are the HRTEM images of the SiC-CDC nano-particles after 24 h, 48 h, and 72 h ECE treatment, respectively. (f) Magnified image of the circled area in (e). The presence of the WG is clearly evident after 72 h ECE technique.

after treated by the ECE technique at a voltage 0.98 V are plotted in Fig. 2a for four treatment periods. Compared to the SiC samples (see Supplementary Fig. S4 online), the SiC-CDC samples showed a much higher electric double layer capacitance. The oxidation peak (Fig. 2a) height and the area beneath the oxidation peak (Fig. 2b) increased with the ECE treatment time up to 48 h, while a surprising decrease occurred after 48 h, which is significantly different from that of Vulcan XC-72 (the amorphous carbon black used in this study) (see Supplementary Fig. S4 online). This area decrease of the oxidation peak indicates an increasing corrosion resistance in SiC-CDC[27].

In order to determine the structural changes of different ECE periods, the HRTEM experiment was conducted. Sporadic graphene fragments appeared on the surface of the SiC-CDC nano-particles after 24 h ECE treatment (Fig. 2c), due to the stripping of the amorphous carbon nano-shell by ECE, which is very different from the SiC-CDC nanoparticles without ECE treatment (Fig. 1b). With ECE treatment, the exposed graphene fragment size became larger and larger. Up to 48 h ECE, the graphene nano-shell was revealed roughly (Fig. 2d). Furthermore, most SiC-CDC nanoparticles were surrounded by more completely wrapped graphene (WG) nano-shell structures after 72 h ECE (Fig. 2 e and f). It can be concluded that the decrease in the area of the oxidation peak is very probably due to the exposing of WG that is larger corrosion resistant than amorphous carbon. In summary, the a-$Si_{1-x}C_x$ nano-shells can be partly transformed into graphene after treating the SiC nano-particles by Cl_2 (Fig. 3). The resulting layered graphene shows at least two different forms, i.e., the EG and WG. The EG formed only on the surface of SiC-CDC nano-particles and some of them can be stripped off, while the WG can only be exposed after removing amorphous carbon using ECE technique.

We further demonstrate the possibility of transforming a-$Si_{1-x}C_x$ nano-films (nano-shells with larger area) on SiC micro-particles into graphene by chlorination. Fig. 4a shows the SiC micro-particle supported a-$Si_{1-x}C_x$ nano-film structures. After chlorination, the a-$Si_{1-x}C_x$ nano-film was transformed into graphene determined by HRTEM (Fig. 4 b, c and d) and Raman spectrum (see Supplementary Fig. S5 online). On the surface of SiC-CDC micro-particle, many detached fine EG (less than ten layers) from SiC-CDC micro-particle, as shown in Fig. 4 c and d, can be easily identified, indicating the relatively weak cohesive strength of the EG/SiC interface, which make it possible to detach EG from SiC surface. In addition, the quality of EG usually shows better quality than other powder-type graphene-materials[11,12], thus separating EG from SiC surface to be "EG powder" becomes an interesting (even important) issue for future applications. Differently, many spherical graphitic layers (not less than ten layers) occur as compared with only presence of few layers graphene nano-sheets on SiC-CDC nano-particles. The presence of graphitic layers is most likely due to the uneven thickness of the a-$Si_{1-x}C_x$ nano-films. For certain regions of a-$Si_{1-x}C_x$ nano-films, the thickness is more than 10 nm (Fig. 4a), which is very different from a-$Si_{1-x}C_x$ nano-shell of SiC nanoparticles (Fig. 1a). Theoretically, the number of graphene layers largely depends on thickness of a-$Si_{1-x}C_x$ nano-film, since the left contents of carbon atom after chlorination determines the number of graphene layers. This gives us a significant clue that only a-$Si_{1-x}C_x$ nano-film which is thin enough could be converted into graphene. Therefore, the number of graphene layers may be controlled by tuning the thickness of a-$Si_{1-x}C_x$ nano-films (shells) or controlling the chlorination process of a-$Si_{1-x}C_x$ nano-film (shells) in the future.

Discussion

At least two possible reasons could be responsible for graphene formation via a-$Si_{1-x}C_x$ nano-shell chlorination. The first is that the amorphous carbon can crystallize into graphene as a result of point defect creation caused by the C atoms consumption. Following the a-$Si_{1-x}C_x$ and β-SiC conversion into the amorphous carbon, the carbon atoms are consumed by reacting with Cl_2 to form the defects continuously[26]. Those defects lower the energy barrier for the conversion from amorphous carbon into graphene. However, Cl_2 almost does not react with C above 600°C[28]. Moreover, according to this hypothesis, the core interface next to the graphene should be made of amorphous carbon due to the preferential combination of Cl_2 with Si atoms[28], this, however, contradicts to our HRTEM results (Fig. 1d).

The second is that a-$Si_{1-x}C_x$ shell can be directly transformed into graphene as a result of a-$Si_{1-x}C_x$ shell etched by Cl_2. According to

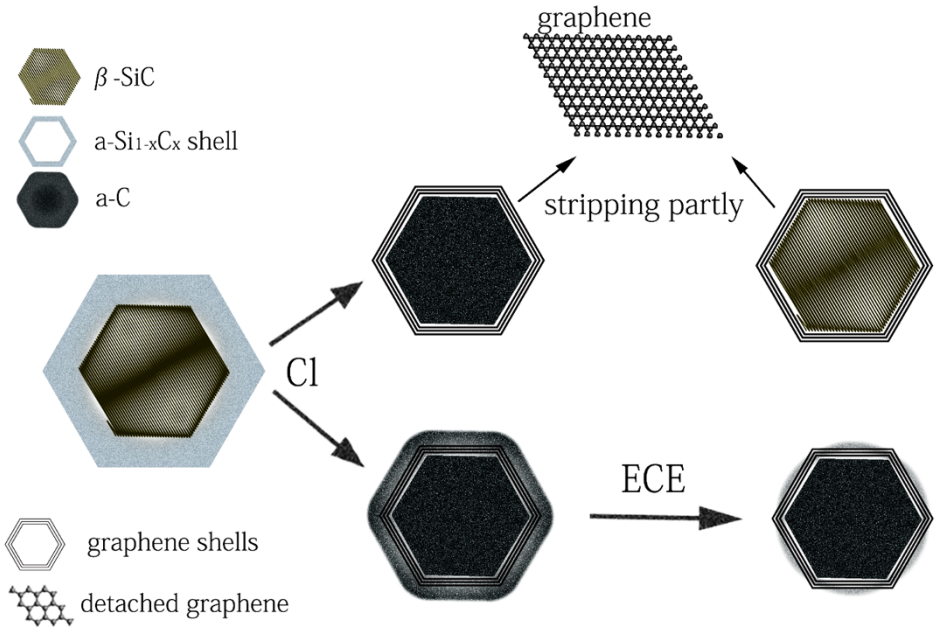

Figure 3 | Schematic of a-$Si_{1-x}C_x$ alloys transformation into three graphene morphologies. The EG and WG processes are shown on the top and bottom, respectively. The EG can be partially stripped off from the surface of SiC-CDC nano-particles. The Cl denotes the chlorination process, and ECE represents the stripping of the amorphous carbon shell via ECE.

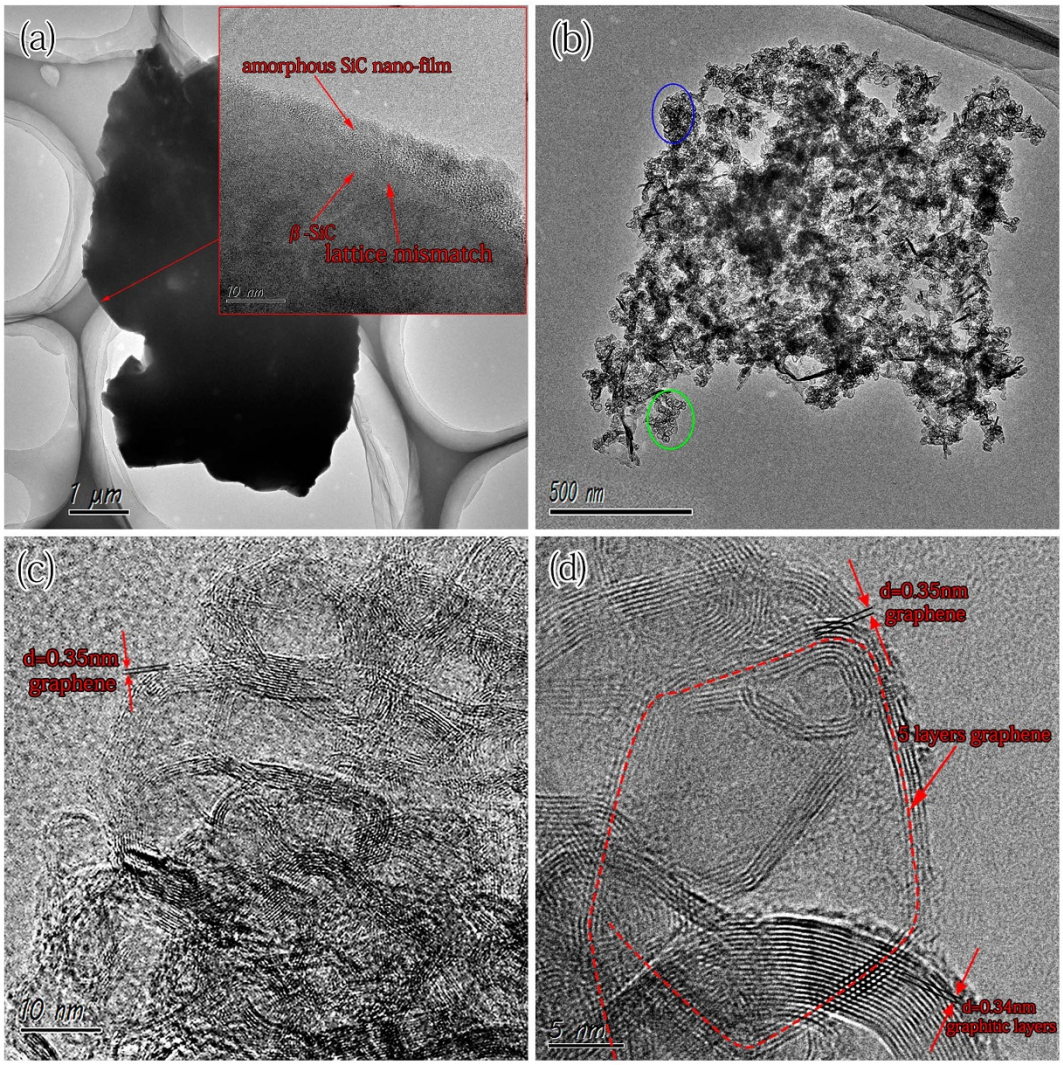

Figure 4 | (a) The HRTEM image of SiC micro-particle. The magnified image shows the a-$Si_{1-x}C_x$ nano-film is on the surface of β-SiC micro-particle. The average particle size of as-received SiC micro-particles is 10 um. (b) The HRTEM image of SiC-CDC micro-particle after SiC chlorination. (c) The magnified HRTEM image of the blue circled area in (b) showing graphene and graphitic layers. (d) The magnified image of the green circled area in (b) showing the graphene and graphitic layers. The common length of resulting graphene is 50–100 nm.

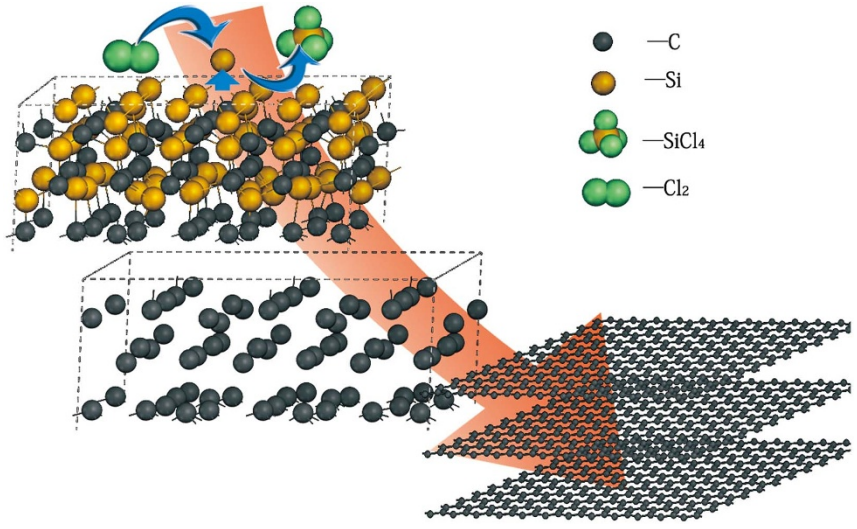

Figure 5 | **Schematic of the transformation of a-$Si_{1-x}C_x$ alloys into graphene.** The long-range disordered a-$Si_{1-x}C_x$ is shown in the upper left, and the Cl_2 react with Si atoms. The middle shows the C rich layers in the intermediate phase after the Si atoms react with Cl_2. The collapsing of C rich layers into the few-layer graphene is shown in the lower right.

our experimental results, the Cl_2 can react with the Si atoms inside the a-$Si_{1-x}C_x$ nano-shell to form thick and highly defective C-rich layers, which subsequently collapse into a thermally stable graphene of few layers (Fig. 5). On the other hand, the ordered graphitic domains in amorphous network of a-$Si_{1-x}C_x$ may act as nuclei for other disordered carbon atoms condensation (see Supplementary Fig. S6 online), promoting the growth of graphene. According to the second hypothesis, the formation of the EGs, including the graphene (Fig. 1 d and e) and the detached graphene (Fig. 1c), can be explained by the conversion of a-$Si_{1-x}C_x$ nano-shell. It is well known that graphene is complete impermeability to any gases[29]. Once continuous graphene layers were formed, they would prevent the SiC from Cl_2 etching, leaving behind β-SiC core (Fig. 1d). While, the formation of graphene layers with break would not provide protection for inner core, thus leaving behind amorphous carbon core (Fig. 1e). For the WG, however, it can be explained by the transformation of the a-$Si_{1-x}C_x$ alloys in the interior of the particle, which can be only exposed after stripping off the amorphous carbon by ECE technique. This mechanism provides a possibility that the transformation result is affected by the x value of a-$Si_{1-x}C_x$. Because the x value is not constant in the a-$Si_{1-x}C_x$ shell, and the a-$Si_{1-x}C_x$ is only transformed into graphene in some special range of x value.

The relatively weak cohesive strength of the EG/SiC interface make it possible to detach EG from SiC surface, thus separating EG from SiC surface to be "EG powder". Firstly, the small size of particles, with higher interfacial free energy, might also play an important role in forming the weak cohesive strength of the EG/SiC interface. However, the quantity of detached graphene from SiC-CDC micro-particles was obviously more than that of SiC-CDC nano-particles. Therefore this mechanism cannot completely explain the HRTEM results (Fig. 1b and Fig. 4b). Alternatively, the lattice mismatch (Fig. 1a and Fig. 4a) between a-$Si_{1-x}C_x$ and β-SiC substrate might give rise to the weak cohesive strength of the EG/SiC interface. Compared with the 6*H*-SiC of whole crystal[11,30], the significant difference between disordered a-$Si_{1-x}C_x$ and ordered β-SiC substrate (see Supplementary Fig. S1 online) results in interface mismatch between a-$Si_{1-x}C_x$ and β-SiC. Then the EG, generated from the a-$Si_{1-x}C_x$ conversion, does not seems to show strong interaction with the β-SiC substrate. While, the graphene, formed on 6*H*-SiC, shows the rotational order relative to the substrate[11,30], which contribute to the relative strong interaction between graphene and 6*H*-SiC.

Meanwhile, there are at least three possible reasons for understanding the much milder conditions in comparison with the extremely harsh conditions used in the SiC crystal annealing process. The first is the long-range disordered lattice of a-$Si_{1-x}C_x$ alloys (see Supplementary Fig. S1 online). Compared with the graphitization of crystal SiC, the graphitization of a-$Si_{1-x}C_x$ alloys skips a redundant step (very high energy barrier) in which the long-range ordered phase is converted into the long-range disordered intermediate phase in graphene formation. The second possibility is the enhanced extraction of Si atom from lattice by Cl_2 etching (Fig. 5) in comparison with the sublimation of Si by high temperature annealing in vacuum or ambient pressure[9,12,31], for the formation of graphene is just the result of Si evaporation from the SiC substrate[12]. The third is probably due to the ordered graphitic domains acting as the nuclei for disordered C atoms condensation during the graphene growth (see Supplementary Fig. S6 online), which can greatly reduce the energy barrier[32].

In summary, we have successfully synthesized the graphene by a-$Si_{1-x}C_x$ chlorination method at the ambient pressure and at a temperature as low as 800°C. The finely epitaxial graphene (EG) can be produced on the SiC nano- and micro-particle, and it might have a relatively low cohesive strength of the graphene/substrate interface. The wrapped graphene (WG) can be well exposed by using the electrochemical erosion (ECE) technique. The chlorination is an economic and scalable method, and the much milder preparation conditions of the method proposed here are more appropriate to large scale manufacturing at low costs, permitting the readily available raw materials and the structural controllability over graphene. Further research will be desirable for a thorough understanding about the influences of the process parameters on the graphene structure and morphology. Especially, the number of graphene layers may be well controlled by applying appropriate process conditions including the x value, the thickness of the a-$Si_{1-x}C_x$ nano-film (shell), and the reaction process.

Methods

The SiC nano- and micro-powders with a-$Si_{1-x}C_x$ nano-shells/films were bought from Kaier Nano Co. and used as-received. The SiC nano- and micro-powders were transformed into the SiC-CDC by selective etching of the Si atoms in chlorine atmosphere at a temperature 800°C via:

$$SiC(s) + 2Cl_2(g) \rightarrow SiC_4(g) + C(s) \quad (1)$$

The SiC nano- and micro-powders were placed into a horizontal hot-wall tubular flow reactor operated at the ambient pressure. The reactor was first filled with pure He gas. Then the reactor was heated up to 800°C under pure He and the samples were exposed to a He/Cl_2 atmosphere for 1 h. The reaction was stopped by flushing the reactor with pure He gas at 800°C for 1 h to remove the residual Cl_2 as well as the by-products from the pores of the samples. Then, the furnace was cooled down to 25°C under pure He. The exhaust gas was neutralized at the reactor exit by bubbling through a 30% KOH solution.

An argon ion laser operated at a wavelength of 514.5 nm was utilized as the excitation light source for Raman analysis. All samples were dispersed ultrasonically in ethanol. An aliquot of this solution was deposited on a carbon film and dried at room temperature. The microstructures of the as-received SiC nano- and micro-powders and the as-prepared SiC-CDC were characterized using JEOL 2010 high resolution transmission electron microscopy (HRTEM). XPS measurements were performed with a VG Scientific ESCALAB 210 electron spectrometer using Mg Kα radiation (hm = 1253.6 eV, 300 W) under a vacuum of 2×10^{-8} Pa. The binding energy was referenced to the C 1 s line at 284.6 eV. The error in the determination of electron binding energies and line widths did not exceed 0.2 eV. The X-ray diffraction (XRD) analysis was performed using a Rigaku X-ray diffractometer equipped with Cu Kα radiation source. The XRD patterns were collected using step scans with a step of 0.01° 2θ and a count time of 2 s per step between 10° and 80° 2θ. The thermogravimetric analysis (TGA) was conducted on an instrument purchased from the TA instruments (NETZSCH STA 449F3). A minimal ambient air flow of 40 ml/min in the temperature range between 100 and 1000°C/min was applied with a heating rate of 10°C/min.

To expose the WG and determine the electrochemical erosion (ECE) rates, a conventional three-electrode electrochemical cell was employed. All the electrochemical measurements were carried out in 0.5 M H_2SO_4 solution at 25°C. The measurements were conducted by using a platinum electrode as the counter electrode and a Hg/Hg_2SO_4 electrode as the reference electrode. For convenience, all potentials measured are referred to as the saturated calomel electrode (SCE).

A polished glassy carbon disk electrode (3 mm diameter) was used as the substrate for the SiC-CDC (or SiC). The working electrode was fabricated as follows: six milligram of the SiC-CDC (or SiC) was dispersed in 1 mL of deionized water and then mixed with 100 uL 5 wt.% perfluorosulfonic acid (PSFA) Nafion (Du Pont Co.) solution. The mixture was sonicated for 6 min to obtain an ink like slurry. Five micro liter of this slurry were spread onto the flat surface of the glassy carbon disk using Finnpipette Digital Micropipette.

The cyclic voltammograms (CVs) and constant-potential acceleration were employed to investigate the ECE rate of SiC-CDC. The SiC substrates were characterized by CVs too. The ECE of SiC-CDC was conducted at a constant potential of 0.98 V over different periods to vary the ECE rates. Meanwhile, the full-scale CVs from −0.22 to 0.98 V were recorded periodically before and after the ECE, in which the constant scan rate was kept at 50 mVs^{-1}. Morphology was examined using the HRTEM after ECE treatment time of 24 h, 48 h and 72 h.

1. Novoselov, K. S. *et al.* Two-dimensional gas of massless Dirac fermions in graphene. *Nature* **438**, 197–200 (2005).
2. Zhang, Y. B., Tan, Y. W., Stormer, H. L. & Kim, P. Experimental observation of the quantum Hall effect and Berry's phase in graphene. *Nature* **438**, 201–2004 (2005).
3. Novoselov, K. S. *et al.* Unconventional quantum Hall effect and Berry's phase of 2π in bilayer graphene. *Nature Phys.* **2**, 177–180 (2006).
4. Novoselov, K. S. *et al.* Room-temperature quantum Hall effect in graphene. *Science* **315**, 1379 (2007).
5. Novoselov, K. S. *et al.* Electric field effect in atomically thin carbon films. *Science* **306**, 666–669 (2004).
6. Eda, G., Fanchini, G. & Chhowalla, M. Large-area ultrathin films of reduced graphene oxide as a transparent and flexible electronic material. *Nature Nanotech.* **3**, 270–274 (2008).

7. Hernandez, Y. *et al*. High-yield production of graphene by liquid-phase exfoliation of graphene. *Nature Nanotech.* **3**, 563–568 (2008).
8. Sutter, P. W., Flege, J.-I. & Sutter, E. A. Epitaxial graphene on ruthenium. *Nature Mater.* **7**, 406–411 (2008).
9. Bolen, M. L., Harrison, S. E., Biedermann, L. B. & Capano, M. A. Graphene formation mechanisms on 4H-SiC(0001). *Phys. Rev. B* **80**, 115433 (2009).
10. Juang, Z. Y. *et al*. Synthesis of graphene on silicon carbide substrates at low temperature. *Carbon* **47**, 2026–2031 (2009).
11. Forbeaux, I., Themlin, J. M. & Debever, J. M. Heteroepitaxial graphite on 6H-SiC (0001): Interface formation through conduction-band electronic structure. *Phys. Rev. B* **58**, 16396–16406 (1998).
12. Emtsev, K. V. *et al*. Towards wafer-size graphene layers by atmospheric pressure graphitization of silicon carbide. *Nature Mater.* **8**, 203–207 (2009).
13. Gogotsi, Y. *et al*. Nanoporous carbide-derived carbon with tunable pore size. *Nature Mater.* **2**, 591–594 (2003).
14. Presser, V., Heon, M. & Gogotsi, Y. Carbide-Derived Carbons – From Porous Networks to Nanotubes and Graphene. *Adv. Funct. Mater.* **21**, 810–833 (2011).
15. banhart, F. & Ajayan, P. M. Carbon onions as nanoscopic pressure cells for diamond formation. *Nature.* **382**, 433–435 (1996).
16. Bullot, J. & Schmidt, M. P. Physics of Amorphous Silicon-Carbon Alloys. *Phys. Stat. Seol. (b)* **143**, 345 (1987).
17. Bechelany, M., Brioude, A., Cornu, D., Ferro, G. & Miele, P. A Raman Spectroscopy Study of Individual SiC Nanowires. *Adv. Funct. Mater.* **17**, 939–943 (2007).
18. Morimoto, A., Kataoka, T., Kumeda, M. & Shimizu, T. Annealing and crystallization processes in tetrahedrally bonded binary amorphous semiconductors. *Philos. Mag. B* **50**, 517–537 (1984).
19. Ferrari, A. C. & Robertson, J. Interpretation of Raman spectra of disordered and amorphous carbon. *Phys. Rev. B* **61**, 14095–14107 (2000).
20. Tuinstra, F. & Koenig, J. L. Raman Spectrum of Graphite. *J. Chem. Phys.* **53**, 1126–1130 (1970).
21. Nemanich, R. J. & Solin, S. A. First- and second-order Raman scattering from finite-size crystals of graphite. *Phys. Rev. B* **20**, 392–401 (1979).
22. Ferrari, A. C. *et al*. Raman Spectrum of Graphene and Graphene Layers. *Phys. Rev. Lett.* **97**, 187401 (2006).
23. Graf, D. *et al*. Spatially Resolved Raman Spectroscopy of Single- and Few-Layer Graphene. *Nano Lett.* **7**, 238–242 (2007).
24. Chen, Z. P. *et al*. Three-dimensional flexible and conductive interconnected graphene networks grown by chemical vapour deposition. *Nature Mater.* **10**, 424–428 (2011).
25. Wei, D. C. *et al*. Synthesis of N-Doped Graphene by Chemical Vapor Deposition and Its Electrical Properties. *Nano Lett.* **9**, 1752–1758 (2009).
26. Tinchev, S. S. Surface modification of diamond-like carbon films to graphene under low energy ion beam irradiation. *Appl. Surf. Sci.* **7**, 2931–2934 (2012).
27. Wang, X., Li, W. Z., Chen, Z. W., Waje, M. & Yan, Y. S. Durability investigation of carbon nanotube as catalyst support for proton exchange membrane fuel cell. *J. Power Sources* **158**, 154–159 (2006).
28. Sui, J. & Lu, J. J. The formation of a dual-layer carbon film on silicon carbide using a combination of carbide-derived carbon process and chemical vapor deposition in a CCl_4-containing atmosphere. *Carbon* **49**, 718–736 (2011).
29. Novoselov, K. S. *et al*. A roadmap for graphene. *Nature* **490**, 192–200 (2012).
30. Emtsev, K. V. *et al*. Interaction, growth, and ordering of epitaxial graphene on SiC{0001} surfaces: A comparative photoelectron spectroscopy study. *Phys. Rev. B* **77**, 155303 (2008).
31. Kim, S., Ihm, J., Choi, H. J. & Son, Y. W. Origins of anomalous electronic structures of epitaxial graphene on silicon carbide. *Phys. Rev. Lett.* **100**, 176802 (2008).
32. Rangappa, D., Murukanahally, K. D., Tomai, T., Unemoto, A. & Honma, I. Ultrathin Nanosheets of Li2MSiO4 (M = Fe, Mn) as High-Capacity Li-Ion Battery Electrode. *Nano Lett.* **12**, 1146–1151 (2012).

Acknowledgements

We gratefully acknowledge support by the National Natural Science Foundation of China (NSFC) (50972112) and the National Basic Research Program of China (973 Program) (2012CB215500). The work carried out at the State Key Laboratory of Advanced Technology for Materials Synthesis and Processing. Thanks to Professor Xueliang Sun of the University of Western Ontario, Canada, for stimulating discussion.

Author contributions

S.M. proposed and supervised the project, T.P. and S.M. designed the experiments, T.P. performed experiments under the help of H.L., D.H., M.P. and S.M. T.P. and S.M. analysed data and wrote the manuscript. All the authors participated in discussions of the research.

Additional information

Supplementary information accompanies this paper at http://www.nature.com/scientificreports

Competing financial interests: The authors declare no competing financial interests.

How to cite this article: Peng, T., Lv, H., He, D., Pan, M. & Mu, S. Direct Transformation of Amorphous Silicon Carbide into Graphene under Low Temperature and Ambient Pressure. *Sci. Rep.* **3**, 1148; DOI:10.1038/srep01148 (2013).